Nuclear Materials and Energy 26 (2021) 100930

Contents lists available at ScienceDirect

Nuclear Materials and Energy

journal homepage: www.elsevier.com/locate/nme

# Global distribution of tritium in JET with the ITER-like wall

S.E. Lee [a], Y. Hatano [a,*], M. Tokitani [b], S. Masuzaki [b], Y. Oya [c], T. Otsuka [d], N. Ashikawa [b], Y. Torikai [e], N. Asakura [f], H. Nakamura [f], K. Isobe [f], H. Kurotaki [f], D. Hamaguchi [f], T. Hayashi [f], A. Widdowson [g], S. Jachmich [h], J. Likonen [i], M. Rubel [j], JET contributors[1]

[a] University of Toyama, Toyama 930-8555, Japan
[b] National Institute for Fusion Science, 322-6, Toki 509-5292, Japan
[c] Shizuoka University, Oya 836, Shizuoka 422-8529, Japan
[d] Kindai University, Kowakae 3-4-1, Higashiosaka 577-8502, Japan
[e] Ibaraki University, Bunkyo 2-1-1, Mito 310-8512, Japan
[f] National Institutes for Quantum and Radiological Science and Technology, Rokkasho 039-3212, Japan
[g] Culham Centre for Fusion Energy, Culham Science Centre, Abingdon, OX14 3DB, UK
[h] Association Euratom-Etat Belge, ERM-KMS, Brussels Belgium
[i] VTT, Otakaari 3J, P.O. Box 1000, FIN-02044, VTT, Finland
[j] KTH Royal Institute of Technology, 100 44 Stockholm, Sweden

A B S T R A C T

Nondestructive analysis of tritium (T) distribution was performed by means of imaging plate technique on specimens cut from the Be limiters, W-coated carbon tiles and bulk W lamellae retrieved from the JET tokamak after the first and third experimental campaigns with the ITER-like wall. Afterwards, analyses were continued using X-ray photoelectron spectroscopy, microscopy techniques and thermal desorption spectroscopy. Co-deposits formed on the W-coated tiles in the 1st campaign showed large T retention because of high carbon content reaching up to 50 atomic %, while the carbon fraction in co-deposits after the 3rd campaign was distinctly lower. The T retention of the plasma-facing surface of the bulk W tile was smaller than that of the W-coated tiles by a factor of 20, while deposition of small amount of T was found at the side surfaces facing to the gaps in a lamella structure. The correlation of T distributions with surface morphology and the discharge conditions is discussed.

## 1. Introduction

ITER will use beryllium (Be) in the main chamber and tungsten (W) in the divertor region as plasma-facing materials [1]. To investigate plasma-surface interactions of these reference materials in tokamak environment, the Joint European Torus (JET) has been operated with the ITER-like wall (ILW): Be limiters and divertor region composed of W-coated carbon fiber composite (CFC) tiles and bulk W lamellae [2]. The JET-ILW campaign started its first operation in 2011 and three consecutive campaigns of deuterium (D) plasma experiments were carried out in 2011–2012 (ILW-1), 2013–2014 (ILW-2) and 2015–2016 (ILW-3) [3,4].

Fuel retention of plasma-facing materials (PFMs) is an important issue controlling tritium (T) inventory in the vacuum vessel. ITER has excluded carbon (C) wall components to avoid the potential risk of rapid accumulation of T by co-deposition with eroded carbon [1]. Indeed, Brezinsek et al. have reported that the long-term D retention in JET with ILW was smaller than that with C wall by an order of magnitude [5]. The distributions of D in the tiles used in ILW experiments have been studied by post-mortem examinations using ion beam analysis, secondary ion mass spectrometry and thermal desorption spectrometry [6–13]. Co-deposition of D with eroded Be and other metallic elements were observed both in the main chamber and the divertor region; thick layers containing D were found at the edges of Be limiter tiles and the W-coated CFC tiles located at the upper-inboard part in the divertor region [3,4,6–13].

Non-destructive determination of the tritium distribution in PFMs has been based on detecting β-rays from T and X-rays induced by the β-rays using imaging plates (IPs) and a silicon-drift detector [14–20]. In JET with ILW, T has been produced as a result of DD fusion reactions (D + D → T [1.01 MeV] + p [3.03 MeV]). The implantation of high energy T (~1.01 MeV) was observed at the plasma-facing surfaces of Be outer limiters [20] and the W-coated CFC tiles located in the upper part of divertor [16]. The co-deposition of T thermalized in plasma with D and

* Corresponding author.
*E-mail address:* hatano@ctg.u-toyama.ac.jp (Y. Hatano).
[1] See the author list of E. Joffrin et al. 2019 Nucl. Fusion 59 112021.

https://doi.org/10.1016/j.nme.2021.100930
Received 25 August 2020; Received in revised form 9 January 2021; Accepted 26 January 2021
Available online 2 February 2021

metallic elements was found mainly in the castellation grooves of Be limiter tiles [20], in the W-coated CFC tiles from the upper-inboard part of diverter and in the shadowed regions of floor tiles [14,15,18]. However, the information on the microstructure of co-deposits and the near-surface regions of substrate tiles was limited, and the mechanisms underlying T retention has not been understood in detail. Only limited data have been obtained for the T distributions in the bulk W tile [19].

Under the framework of Japan-EU Broader Approach DEMO Research and Development activities, samples cut from the Be limiter tiles, W-coated CFC tiles and bulk W lamellae retrieved after ILW-1 and ILW-3 were shipped for post-mortem analyses to the International Fusion Energy Research Centre (IFERC), National Institutes for Quantum and Radiological Science and Technology (QST), Rokkasho, Japan. The samples were first subjected to nondestructive analyses of T distributions using the IP technique and β-ray induced X-ray spectrometry (BIXS). Then, the samples were cut into four equal pieces to perform analyses using X-ray photoelectron spectroscopy (XPS), transmission electron microscopy (TEM) and T measurements using thermal desorption spectroscopy (TDS). The results of these nondestructive and destructive analyses are summarized in this paper for deeper discussion on the correlation of T distributions with the microstructures and the discharge conditions. In addition, the T distributions in the bulk W tile are also reported in detail.

## 2. Experimental procedures

The samples listed in Table 1 were prepared from the Be tiles, the W-coated CFC tiles and the bulk W lamella tile and then shipped to IFERC. The Be tiles examined were retrieved from the midplane positions and upper part of the main chamber of JET after ILW-1 and ILW-3 (Fig. 1). Those tiles are described as inner wall guard limiter (IWGL), outer poloidal limiter (OPL) and dump plate (DP). The W-coated CFC tiles and bulk W lamella tile were located in the divertor region, as shown in Fig. 1. The detailed structure of the bulk W lamella tile is given in Fig. 2 [19]. The W-coated CFC tiles were retrieved after ILW-1 and ILW-3, while the bulk W lamella tile was taken out after ILW-1. To ensure their durability under severe heat loads, all bulk Be tiles are castellated: 12 × 12 mm net with a 12 mm deep and 0.4 mm wide grooves. Several castellation sections were cut from the above-mentioned tiles, as shown in Fig. 3. Three samples (10 × 9 × 6 mm) were taken from the bulk W lamella tile, as shown in Fig. 2. Disk samples (17 mm diameter and 5 mm thickness) were prepared from the W-coated CFC tiles at the positions indicated by black dots in Fig. 1 (see also Fig. 7). The thickness of W coating was 10–20 μm. The plasma-facing surface of Tile 3 used in ILW-1 was covered by Mo layer instead of W layer to enable the investigation of W deposition [17].

As described earlier, T in JET is generated by DD fusion reactions. A part of T is thermalized in plasma, while a remaining part is implanted into the tiles at high energy up to 1.01 MeV depending on the collision in the plasma. The simulation using SRIM code [21] indicated that the range of 1.01 MeV T at normal incidence is 10.6 μm in Be and 4.6 μm in W.

**Table 1**
Summary of the tile samples examined in this study. The numbers inside parentheses are castellation numbers for Be tiles, sample numbers for W-coated CFC and bulk W tiles.

| | ILW-1 | ILW-3 |
|---|---|---|
| Castellation samples from Be limiter tiles | IWGL 2XR10 (13, 36), OPL 4D14 (123, 127, 160), DP 2BC2 (78, 87) | IWGL 2XR10 (491), OPL 4D14 (556, 560), DP 2BC2 (447, 456) |
| Disk samples from W coated CFC tiles | Tile 1 (10, 8, 5, 2), Tile 3 (6, 4, 2), Tile 4 (10, 7, 6, 1), Tile 6 (2, 6, 9), Tile 7 (1, 5, 8), Tile 8 (1, 5, 8, 10) | Tile 1 (10, 8, 6, 2), Tile 3 (6, 4, 2), Tile 4 (10, 7, 6, 1), Tile 6 (2, 6, 9), Tile 7 (1, 5, 8), Tile 8 (1, 5, 8, 10) |
| Lamella samples from bulk W tile | Tile 5, Stack C (C3, C22, C23) | |

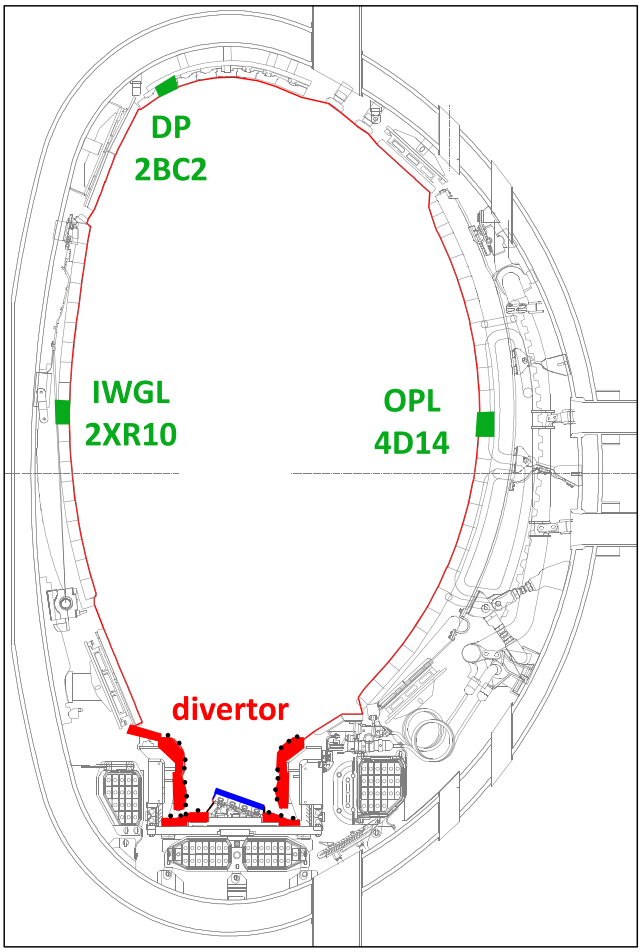


**Fig. 1.** Cross-sectional view of JET vacuum vessel and positions of the tiles examined in this study. Green squares in the main chamber indicate Be limiter tiles: inner wall guard limiter (IWGL), outer poloidal limiter (OPL) and dump plate (DP). Red lines in the divertor region shows the positions of W-coated carbon fiber composite (CFC) tiles, and blue line indicate the position of bulk W lamella tile (Tile 5). Black dots on the W-coated CFC tils indicate the positions from where the disk samples were prepared. (For interpretation of the references to colour in this figure legend, the reader is referred to the web version of this article.)

Two types of IPs were used. One is BAS-TR type (Fujifilm, Japan). This type of IP has 50 μm-thick phosphor coating without any protection layer and sensitive to low energy (≤18.6 keV) β-rays from T. The other is BAS-MS type (Fujifilm, Japan) having 115 μm-thick phosphor layer covered by 9 μm-thick plastic layer for protection of hygroscopic phosphor. The latter was used to examine the intensity of X-rays induced by β-rays from T. In contrast to BAS-TR, BAS-MS is insensitive to β-rays from T because the β-rays are fully attenuated in the plastic protection layer. From the equation proposed by Katz and Penfold (Eq. 8 in [22]), the escape depths of β-rays in W, Be and BeO were evaluated to be 0.3, 3 and 2 μm, respectively. The X-ray spectra induced by β-rays from T extend over 0–10 keV [16]. From the mass attenuation coefficients for W, Be and O [23], the escape depth of 5 keV X-rays was evaluated to be 2 μm in W, 2800 μm in Be and 280 μm in BeO. Here, the escape depth is defined as material thickness by which the intensity of X-rays is attenuated to 1/10. The β-ray IP (BAS-TR) is suitable to evaluate distributions of T on/near the surface of tiles such as T retained in the co-deposits. The X-ray IP was used to study the distribution of T retained in the deeper regions of the tiles.

The samples were put in the darkroom on IP together with a set of

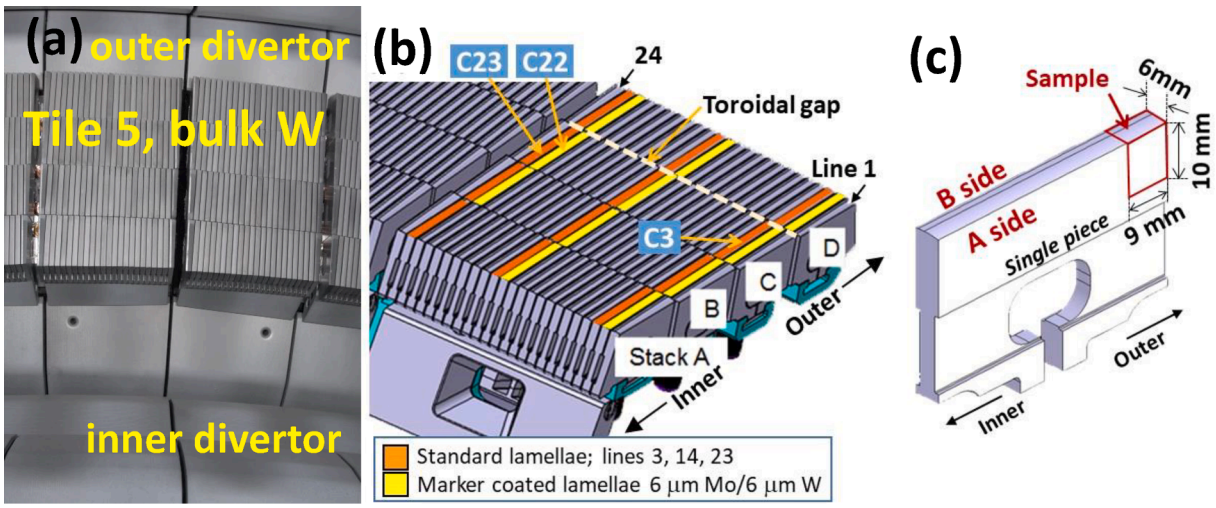


**Fig. 2.** (a) Photo of Tile 5 (bulk W lamellae tile) in the vacuum vessel, (b) entire CAD image of Tile 5, and (c) CAD image of a single piece of W lamella. A side is the ion drift side and B side is the electron drift side. [Reproduced from M. Tokitani et al., Surface morphology of the bulk tungsten divertor tiles from JET ITER-like wall, Phys. Scr. T171 (2020) 014010, doi: https://doi.org//10.1088/1402-4896/ab3d09.]

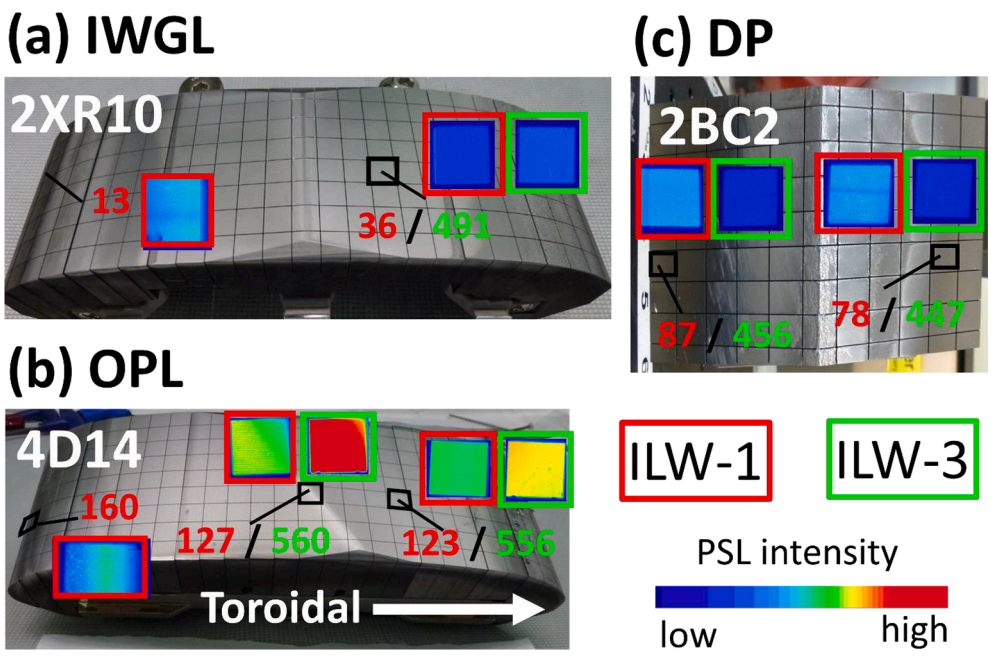


**Fig. 3.** Beryllium limiter tiles and 2-dimensional β-ray images taken by using imaging plate. The β-ray images were prepared using an exponential scale mode of the Multi Gauge software (Fujifilm Co., Japan). Colors indicate the intensity of photo-stimulated luminescence (PSL) from imaging plates in descending order from red (highest), yellow, green and blue (lowest). Red and green frames and numbers indicate samples from ILW-1 and ILW-3, respectively. (For interpretation of the references to colour in this figure legend, the reader is referred to the web version of this article.)

reference plastic samples labelled with known amounts of tritium: ART0123A, American Radiolabeled Chemicals, USA. The T concentrations in the plastic samples ranged from 74 Bq/mg to 273 kBq/mg on the calibration day (July 2014). The actual T concentrations on the measurement days were evaluated from the half-life of T (12.3 years). The density of the plastic samples was about 1 g/cm$^3$. The exposure time was around 20 h for β-ray measurements and 69–164 h for X-ray measurements. Using a laser scanner (FLA-7000, Fujifilm, Japan) 2-dimensional (2-D) distributions of photo-stimulated luminescence (PSL) were obtained.

After the IP measurements, the disk samples taken from the W-coated CFC tiles were cut in 4 equal pieces using a precision sectioning saw in air without a lubrication fluid. T retention in selected sample pieces were evaluated using TDS [24,25]. The sample was heated in a quartz tube evacuated by a turbomolecular pump and a scroll pump to 1273 K at a ramp rate of 0.5 K/s. T contained in the exhaust gas from the scroll pump was oxidized to HTO/DTO and trapped in a water bubbler. The amount of trapped T was evaluated using a liquid scintillation counter. Additional analysis using XPS and TEM were also performed. Samples for TEM were prepared with a focused ion beam (FIB) machining in a manner described elsewhere [19,26,27].

As summarized in Table 1 in [20], the total number of shots was 3668 and input energy was 145 GJ in ILW-1. The total times of limiter plasma and divertor plasma were 7.76 and 12.62 h, respectively. In the case of ILW-3, the total number of shots was 4420 and input power was 245 GJ. The total times of limiter plasma and divertor plasma were 4.86 and 18.47 h, respectively. It should be noted that the ratio of limiter-to-divertor operation was distinctly different in the two campaigns: 0.61 and 0.26 in ILW-1 and ILW-3, respectively. The larger total number of shots and input energy in ILW-3 should result in production of larger amount of T by DD reactions. Indeed, the amount of produced T evaluated from neutron measurements was 15 GBq in ILW-1 and 40 GBq in ILW-3.

## 3. Results and discussion

### 3.1. Be limiter tiles retrieved from main chamber

Fig. 3 shows Be tiles and 2-D β-ray images of plasma-facing surfaces of Be limiter tiles. The β-ray images were prepared using an exponential scale mode of the Multi Gauge software (Fujifilm, Japan). The colors indicate the intensity of PSL in the descending order from red (highest), yellow, green and blue (lowest). The red and green numbers in the images denote respective samples (single castellation blocks) from ILW-1 and ILW-3, respectively. The highest level of PSL intensity is at the central part of OPL (Sample 127 and 123 for ILW-1 and 560 and 556 for ILW-3). The edge of OPL (Sample 160), IWGL (Sample 13, 36 and 491) and DP (Sample 78, 87, 447, 456) show far lower PSL intensity.

As reported in [3,4], the central part of OPL was an erosion-dominant zone, while the deposition of metallic elements and D were observed at the edges. The enrichment of T at the erosion-dominant zone suggests that the main mechanism of T retention for the Be tiles is the implantation of high energy T (~1.01 MeV). The analysis of spectra of β-ray induced X-rays by Monte Carlo simulation in our previous study showed that the penetration depth of T into Be tiles was ~6 μm after ILW-1 [20]. The X-ray measurements and analysis performed for the Be tiles retrieved after ILW-3 in the same manner indicated the comparable penetration depth of T (~6 μm).

Fig. 4 shows the T retention of Be tiles evaluated by comparing the PSL intensity with that of the plastic reference samples on the assumption that the density of the tile is the same as metallic Be (1.85 g/cm$^3$) and the escape depth of β-rays is inversely proportional to the density of the materials. The T penetration depth was set to be 6 μm. The central part of OPL showed orders of magnitude larger T retention than IWGL and DP. The T retention after ILW-3 was larger than that after ILW-1 for OPL and IWGL, while DP showed opposite tendency. The intervals between the end of experimental campaigns in JET and T analysis were about 6 years for ILW-1 Be tiles and 3.5 years for ILW-3 Be tiles. During these intervals, the amount of T was reduced to ~ 70% of the initial value for ILW-1 tiles and ~ 82% for ILW-3 tiles by decay to $^3$He. The difference in the interval was too small to explain the difference in T retention between ILW-1 and ILW-3 observed in Fig. 4. As described earlier, the amount of T produced in ILW-3 was larger than that in ILW-1. Hence, it is plausible that a larger amount of T was implanted into the tiles. In addition, as previously mentioned, the limiter plasma time was shorter in ILW-3 than ILW-1. Hence, the OPL and IWGL used in ILW-3 were less eroded than those used in ILW-1. It is probable that the larger T retention after ILW-3 was caused by the combination of a larger amount of implanted T and less T removal by erosion. As discussed in [20], the T retention in DP cannot be explained simply by implantation and erosion because DP tiles received a large amount of energy (~MJ) in disruptions [28]. Fig. 13 in [28] shows that the number of disrupted pulses providing high energy to the particular DP tile examined in this study (DP2, the second tile from the inboard side) was larger in ILW-3 than in ILW-1. This may be one of the causes of smaller T retention observed for DP after ILW-3 than ILW-1. Pajuste et al. [29,30] examined T retention in Be tiles by acid dissolution method and TDS and observed the largest retention at the central part of OPL. Data obtained in the current work are consistent with those results.

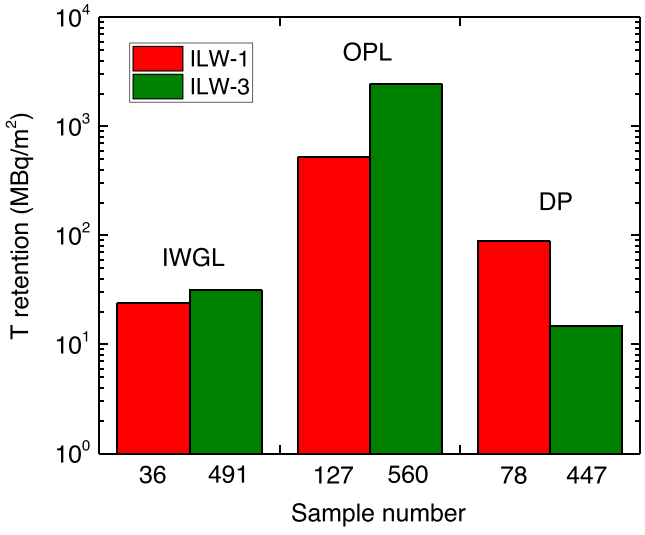


**Fig. 4.** Tritium retention of Be tiles evaluated from PSL intensity by assuming the penetration depth of T is 6 μm [20].

Fig. 5 shows TEM image of lamellae sample taken from OPL sample (Sample 123) by FIB machining in a direction perpendicular to the plasma-facing surface. In other words, this figure shows the cross-sectional image of the region near the plasma-facing surface of Sample 123. The elemental maps were also acquired using energy dispersive X-ray spectroscopy (EDS), as shown at the bottom of Fig. 5. Small particles enriched with O and N have been detected. One may suggest that these are precipitates of Be oxide, nitride and/or oxynitride. As mentioned previously, Sample 123 showed relatively large T retention. The understanding of the roles of these particles in T trapping is an important issue for the clarification of mechanisms underlying the large T retention in the central part of OPL.

The T distributions on castellated surfaces were also analyzed using β-ray IP from the entrance of the castellation groove (0 mm) to deeper region (up to 8 mm), as shown in Fig. 6. The side surfaces of Sample 36 and 491 from IWGL, Sample 123 and 556 from OPL and 87 and 456 from DP were examined. Near the entrance (~2 mm), T concentration was high and varied depending on the position of the tile in the tokamak. The highest concentration was found in OPL and it corresponded to the largest T retention in the plasma-facing surface. In the deeper region, the difference between the samples was smaller. Rubel et al. [10] have examined distributions of D and metallic impurities in the castellation grooves and found graded concentration profiles of D and metallic elements extended to ~ 1–3 mm from the entrance to the gap. The observation in this study is consistent with the results reported by Rubel et al [10]. This agreement suggests that the main mechanism underlying T retention on the castellation surfaces is co-deposition with D and metallic elements including Be. In the cases of IWGL and DP, the concentration after ILW-3 was less than half of that after ILW-1. As described earlier, the erosion of plasma-facing surfaces in ILW-3 is expected to be less than that in ILW-1. In addition, as reported in [4], the difference between ILW-3 and ILW-1 in the duration of plasma contact with limiters was larger for IWGL than for OPL. The less erosion of plasma-facing surfaces should result in less deposition of Be in the grooves and consequent smaller T retention. The smaller T retention on the castellation surface of DP after ILW-3 can be ascribed to the higher heat load, as discussed earlier.

### 3.2. Divertor tiles

#### 3.2.1. Plasma-facing surfaces

Fig. 7 shows the cross-sectional image of JET divertor region together with 2-D β-ray images of the plasma-facing surfaces of the tiles. The round images correspond to the disk samples taken from the W-coated CFC tiles, while the square image between Tile 4 and Tile 6 corresponds to Sample C3 cut from Slack C of Tile 5. The β-ray images were prepared using an exponential scale mode of the Multi Gauge software. The inner and outer strike points were predominantly on the surfaces of inner vertical tile (Tile 3) and that of bulk W tile (Tile 5), respectively, in ILW-1, as indicated by green lines in the figure. During ILW-3, the strike points were mainly on the corners of inner floor tile (Tile 4) and outer floor tile (Tile 6), as marked by blue lines. Square contrasts at the upper part is the images of plastic reference samples labelled with known amounts of T. Fig. 8 shows the average PSL

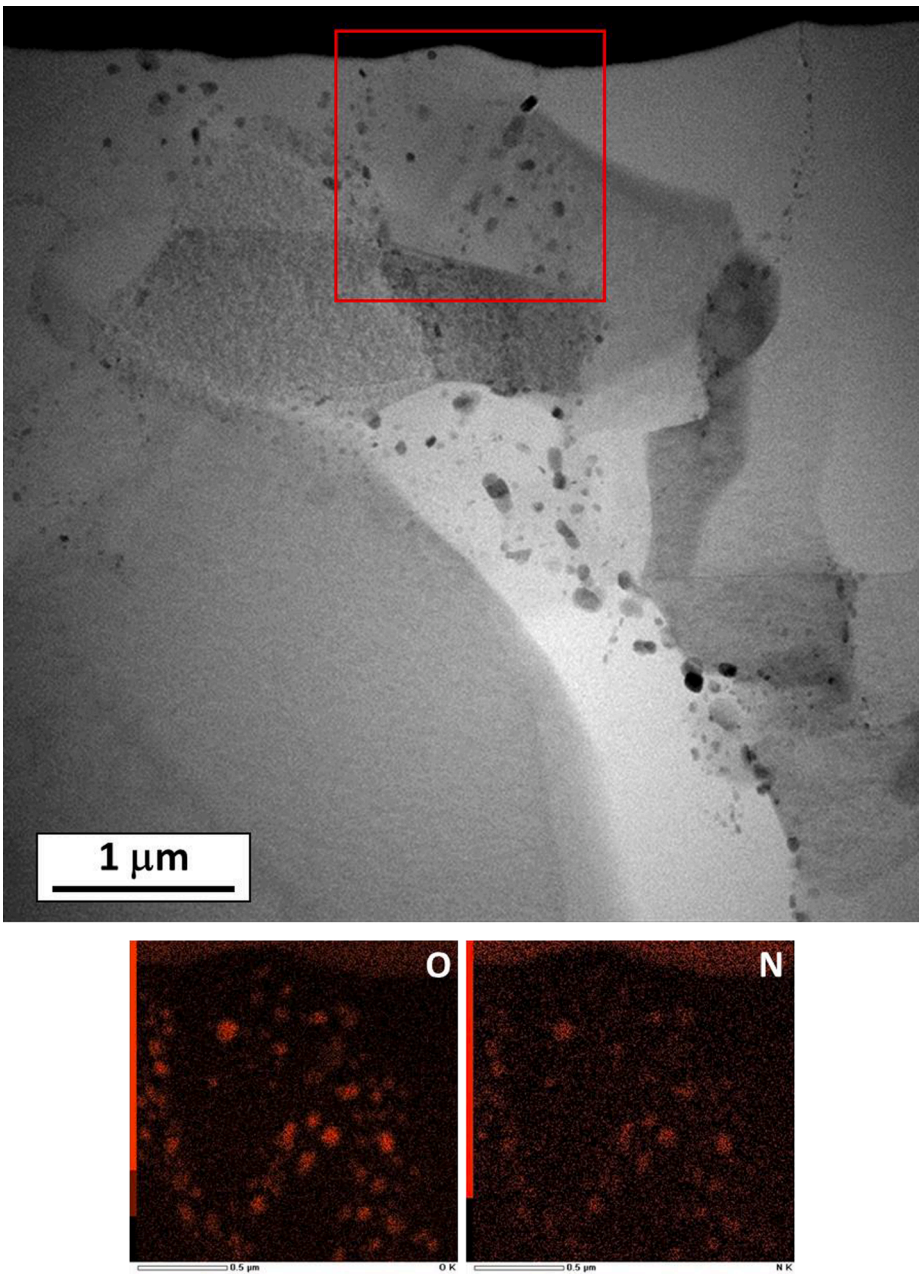


**Fig. 5.** Bright field image of lamella sample prepared by FIB machining from Be tile Sample 123 in the direction perpendicular to the plasma-facing surface (top) and element distributions obtained by EDS from the region indicated by red square in the bright field image (bottom). (For interpretation of the references to colour in this figure legend, the reader is referred to the web version of this article.)

intensity for each sample; the values shown in this figure were normalized by the PSL intensity of the plastic reference sample indicated by the white arrow in Fig. 7. The characteristic points of these two figures are:

(1) The PSL intensities for the inboard tiles are higher than those for the outboard tiles;
(2) Sample 4–10 after ILW-1 shows outstandingly high PSL intensity; the intensity of this sample is higher than the average intensity of other ILW-1 tiles by a factor of ~ 15.
(3) Tile 3 and Tile 6 show higher PSL intensity after ILW-3 than ILW-1;
(4) The PSL intensities for the Tile 5 samples are very low: ~1/20 of the average intensity of the W-coated CFC tiles.

The intervals between the end of experimental campaigns in JET and T analysis were about 3.3 years for ILW-1W-coated CFC tiles and 2.3 years for ILW-3 tiles. During these intervals, the amount of T was reduced to ~83% of the initial value for ILW-1 tiles and ~88% for ILW-3 tiles by decay to $^{3}$He. Again, the difference in the interval was too small to explain the difference in T retention between ILW-1 and ILW-3 observed in Figs. 7 and 8.

It has been found that relatively thick co-deposits were formed on the surfaces of Tile 0 and 1, and shadowed regions of Tile 4 and 6 [6–9]. The plasma-facing surfaces of Sample 1–10 and 4–10 were covered by co-deposition layer of mixed material (W, C, O, Mo and Be) with thickness of ~ 10 μm [8] and 200–300 nm [26], respectively. In contrast, no remarkable surface modification was observed for the samples from Tile 7 and 8 [27]. Hence, the higher PSL intensity observed for the inboard tiles was attributed to co-deposition of T thermalized in the plasma with

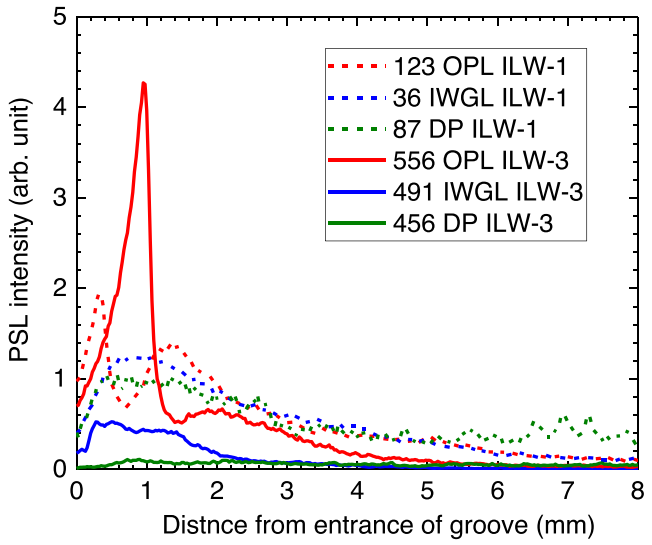


**Fig. 6.** Tritium profiles on the side surfaces facing the castellation grooves of Be tiles.

Be and other impurities. As reported in the previous papers, T-enriched band-like regions extended in the toroidal direction were observed for divertor tiles after ILW-1 and ILW-2 [14,15,18]. These band-like regions corresponded to the areas covered with relatively thick co-deposits. The XPS analysis performed by Oya et al. [24] showed the presence of hydroxides (M(OH)$x$ where M is a metallic element, H indicates all hydrogen isotopes, and $x$ is the fraction of OH to the metallic element). It is possible that some fraction of T was present in the form of OH.

Sample 4–10 after ILW-1 was located in one of the such band-like regions. The high PSL intensity observed for this sample indicates high T fraction in the co-deposited layer. XPS examination [25] of co-deposits indicated that the carbon content on Sample 4–10 was significantly higher than other samples. As shown in Fig. 4 in [25], the surface layer of ILW-1 Sample 4–10 contained Be 25–30%, C 50–30%, O 25–35% depending on depth, while that on Sample 1–6 was Be: ~45%, C ~ 10% and O ~ 45%. Mayer et al. have examined distributions of Be, D and C on divertor tiles after ILW-2 using ion beam techniques [9] and also observed high C/Be and D/Be rations at the shadowed region of Tile 4. Therefore, the outstandingly high T concentration in the co-deposit on ILW-1 Sample 4–10 can be attributed to the high C fraction in the co-deposit. The T concentration in the co-deposit on Sample 4–10 after ILW-1 was evaluated to be ~ 10–20 MBq/cm$^3$ [14]. It should be noted here that the retention of T is determined by the product of fraction of T in the analyzed layer and the thickness of that layer. Hence, the T retention of Sample 1–10 could be higher than that of Sample 4–10 due to the thicker co-deposit, as observed for D [25]. The XPS analysis showed significantly lower C fraction in the layers formed on the inner divertor tiles after ILW-3 [25]. The reduced C fraction in the co-deposits can be the cause of the absence of area with outstandingly high PSL intensity after ILW-3.

The higher PSL intensity of inner vertical tiles (the vertical part of Tile 1 and Tile 3) after ILW-3 than after ILW-1 can be explained by the difference in the inner strike point. As previously mentioned, the inner strike point was predominantly located on Tile 3 in ILW-1 and on Tile 4 in ILW-3. It means the heat load for inner vertical tiles was lower in ILW-3 than ILW-1. Consequently, more T remained in the tiles.

The outer strike point was predominantly located on Tile 5 in ILW-1. The microstructure analysis of Sample C3, C22 and C23 revealed that the plasma-facing surfaces of these samples were eroded by plasma and the microstructures in the subsurface regions were significantly modified by heat and particle loads [19]. The very low PSL intensity for Tile 5 samples were ascribed to the removal of T by erosion and thermal desorption.

Fig. 9 shows the distribution of PSL intensity from X-ray IP (BAS-MS) after the contact with the disk samples from the W-coated CFC tiles retrieved after ILW-1 and ILW-3 (a) together with the T retention in the sample pieces evaluated using TDS (b). The signal intensities from Tile 5 (W lamellae tile) samples were comparable with the background level and therefore not shown in the figure. The characteristic points of this figure are: (i) the difference between inboard side and outboard side was clearly smaller than the case of β-ray IP (Fig. 8); and (ii) the T retention after ILW-3 was larger than that after ILW-1.

As described earlier, β-ray IP mainly detects T retained in the co-

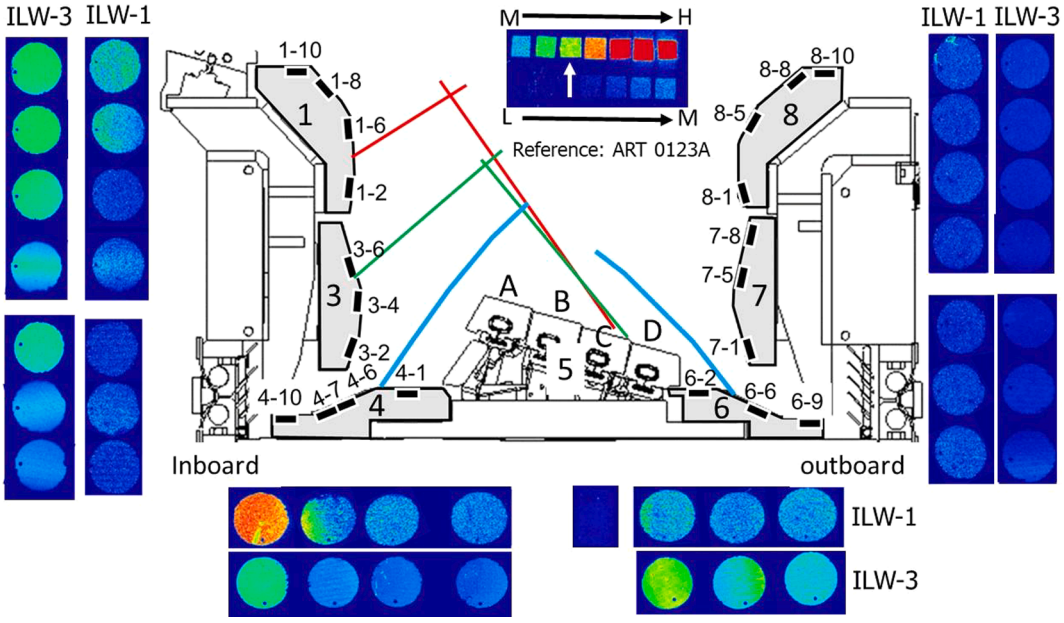


**Fig. 7.** Cross-sectional view of divertor region of JET together with 2-dimensional β-ray images of disk samples cored from W-coated CFC tiles (Tiles 1, 3, 4, 6, 7 and 8) and sample taken from W lamella tile (Tile 5, Stack C, C3 lamella). Square contrasts at upper part are images of plastic reference samples labelled with known amount of T. H, M and L indicate high, medium and low T concentration, respectively. Lines in red, green and blue colors indicate typical strike point positions during JET operation. (For interpretation of the references to colour in this figure legend, the reader is referred to the web version of this article.)

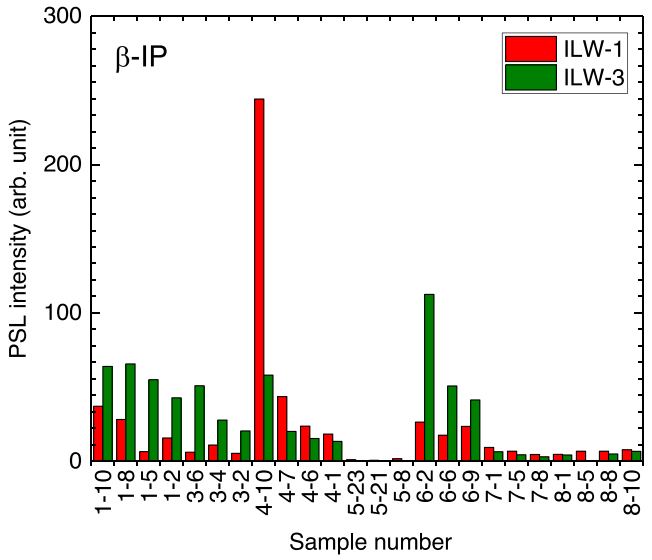


**Fig. 8.** Intensity of photo-stimulated luminescence (PSL) after exposing imaging plate to β-rays from samples taken from divertor tiles. See Figs. 1, 2 and 7 for locations of samples in the tokamak.

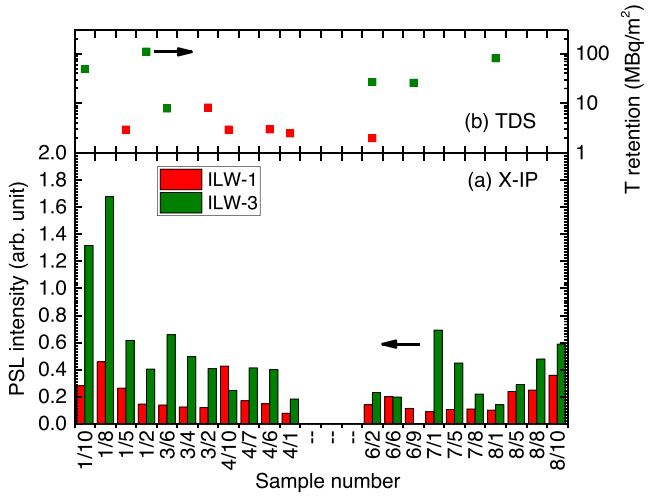


**Fig. 9.** (a) Intensity of photo-stimulated luminescence (PSL) after exposing imaging plate to X-rays from samples taken from divertor tiles, and (b) T retention evaluated by thermal desorption spectrometry. See Figs. 1 and 7 for locations of samples in the tokamak. The signal intensities from Tile 5 (W lamellae tile) samples were comparable with the background level and therefore not shown in the figure.

deposited layers. The difference between β-ray IP and X-ray IP indicates the presence of T beyond the escape depth of β-rays. A part of T produced by DD reactions is implanted into the tiles at high energy up to 1.01 MeV. This implantation of high energy T should be the cause of presence of T in the deeper region. The analysis of X-ray spectra performed in the previous study for the tiles retrieved after ILW-2 also confirmed the penetration of T into the W coatings up to the depth of several micrometers [16]. Relatively uniform distributions of X-ray intensity and T retention evaluated using TDS indicate that the fluence of high energy T to the inboard side and that to the outboard side were comparable with each other. The larger T retention after ILW-3 was also confirmed by T measurements using a combustion method [31]. These observations are consistent with the above-mentioned results of neutron measurements indicating that the amount of T produced in ILW-3 was larger than that in ILW-1. The results obtained by means of a combustion method will be reported in a separate paper.

To examine whether the penetration of T through W coatings to the CFC substrate occurred, the cross-sectional surfaces and backside surfaces formed by cutting was also subjected to the analysis with β-ray IP. The PSL intensity for the cross-sectional and backside surfaces was below the detection limit. The plastic reference samples showed that the detection limit of this measurement was ~ 10 kBq/g. Hence, even in the case the penetration happens, the T concentration in the CFC substrate was less than ~ 10 kBq/g. In addition, these observations suggest that the cross contamination during cutting was negligible.

Post-TDS analysis were performed using β-ray IP to examine the amount of T remaining after the heat treatment at 1273 K in a vacuum. The PSL intensity obtained after TDS was comparable with a background level for all measured samples except ILW-1 Sample 4–10. Sample 4–10 showed meaningful intensity of PSL even after the TDS measurement, and it was 1% of the intensity before the TDS measurement. In other words, 1% of T remained in the co-deposit after the heat treatment at 1273 K in a vacuum. This observation can also be explained by the high C fraction in the layer.

Results in Figs. 7 and 8 show that the C fraction in co-deposits is a key factor influencing the T retention. Formation of C-dominant layer is observed even in a fusion device with full metallic walls. A spherical tokamak in Kyushu University, QUEST, has stainless steel and W walls, and this device has never been operated with C wall [32]. However, the formation of carbon deposition layer and its influence of hydrogen retention were observed [32]. During successive experimental campaigns, the fraction of C in the co-deposits gradually decreased, while that of metallic elements (Fe, Cr, Ni and W) increased [33]. It is important in ITER operation to reduce sufficiently the content of C impurity in a vacuum vessel before starting DT experiments.

### 3.2.2. *Poloidal and toroidal gap surfaces of Tile 5 samples*

Fig. 10 shows appearance and 2-D β-ray maps of (a) plasma-facing surfaces, (b) ion drift side (A side in Fig. 2) and (c) electron drift side (B side in Fig. 2) of poloidal gap surfaces, and (d) toroidal gap surfaces of samples from Tile 5 (W lamellae tile). The outboard side is in the right side in the row (b), and in the left side in the row (c). The β-ray images were prepared using a linear scale mode of the Multi Gauge software. $B_t$ means toroidal magnetic field. Black contrasts indicated by red circles in the photos are C dots intentionally put on the samples as position markers and they have no further scientific meaning.

As previously mentioned, T retention on the plasma-facing surfaces of Tile 5 samples was 1/20 of that on the W-coated CFC tiles. On the other hand, clearly higher T retention was observed on the poloidal and toroidal gap surfaces. The area with high T retention corresponded to the regions with dark contrasts in the photos. The microstructural analysis previously performed by using electron probe microanalyzer showed that the dark contrasts were formed by deposition of mixed materials of Be and O [19]. XPS analysis of the dark area showed that some oxygen was present as OH. Hence, it can be considered that T was retained in the co-deposits and a certain fraction of that isotope could be in the form of OT. Indeed, the signal intensity dropped to the background level by removal of co-deposits via sputtering in the XPS device. The thickness of the layer formed on the toroidal gap surface of Sample C22 was 300–600 nm, and the T retention in that layer could be estimated at the level of 40 kBq/cm$^2$ using the plastic reference samples by taking into account of the difference in density [19]. The T retention on poloidal gap surfaces of Sample C23 was larger than those of C22 and C8. Due to the geometry of the tiles, the lamellae C23 and adjacent C24 received highest heat and particle influx during operation [19]. The largest T retention can be connected with highest particle influx to that part of Tile 5. For all samples examined, no systematic difference between ion drift side and electron drift side was observed, while T retention at the outboard side was higher than that at the inboard side. These observations suggest that the direction of plasma influx and the shadowing effects caused by the geometry of plasma-facing component

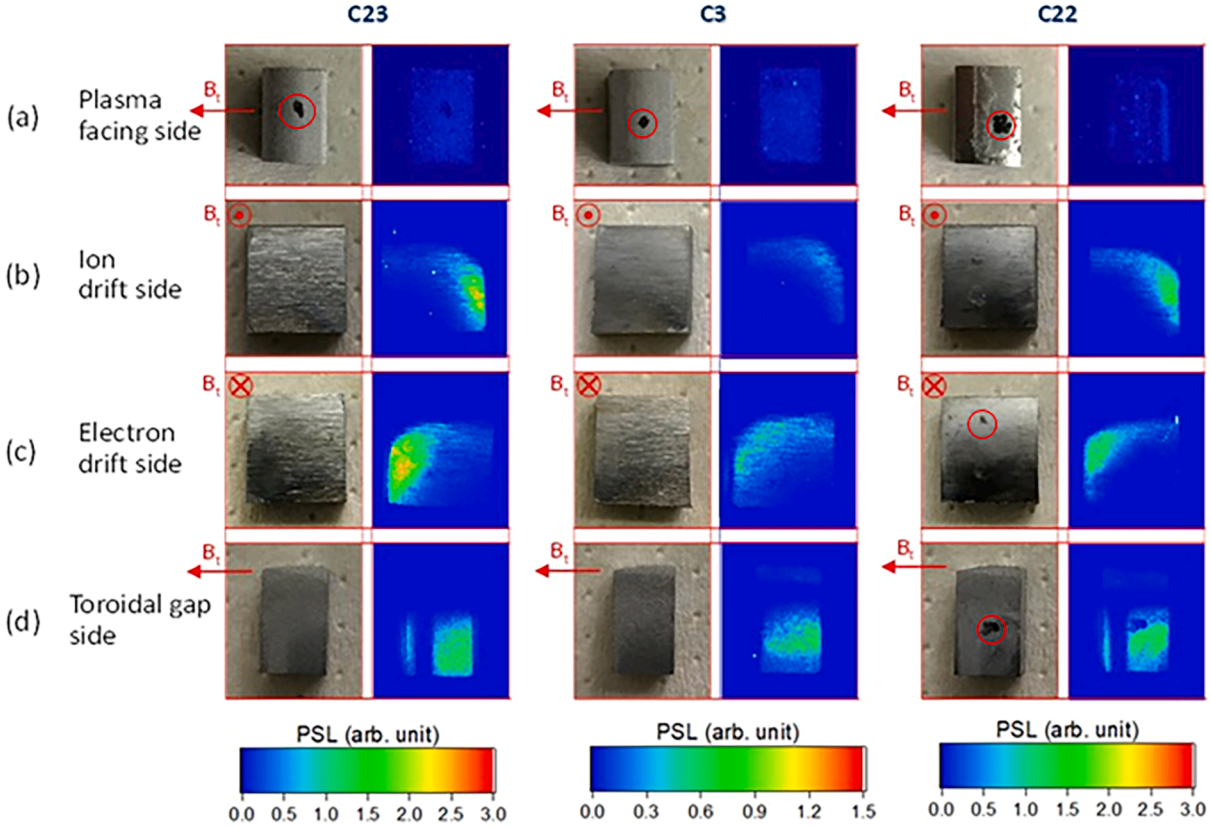


**Fig. 10.** Photos and 2-dimensional β-ray images of (a) plasma-facing surfaces, (b) and (c) poloidal gap surfaces, and (d) toroidal gap surfaces of samples taken from Tile 5 (W lamellae tile). The outboard side is in the right side in the row (b), and in the left side in the row (c). $B_t$ means toroidal magnetic field.

can have strong impact on T distribution.

## 4. Conclusions

(1) The central part of OPL showed the largest T retention in the plasma-facing surfaces of the Be limiter tiles in the main chamber. The erosion was dominant over the deposition in this region, and hence the large T retention was explained by the implantation of high energy T (up to 1.01 MeV) produced by DD fusion reactions. The cross-sectional TEM observation of the subsurface region showed the presence of nanoparticles enriched with N and O. Understanding of the influence of these impurities on T retention is a future task.

(2) The deposition profiles of T in the castellation grooves of the Be limiter tiles after ILW-3 were similar to those after ILW-1; The large T retention at 1–2 mm depth from the entrance of grooves was observed together with the gradual decrease with increasing depth in the deeper region. The variation in T retention was explained by the difference in discharge conditions between ILW-1 and ILW-3.

(3) In the divertor region, the T-containing co-deposits were preferentially formed on the W-coated CFC tiles located at the upper-inboard region (Tile 1) and shadowed regions of floor tiles (Tile 4 and Tile 6). The implantation of high energy T occurred more uniformly. Hence, the difference between inboard side and outboard side in T retention was smaller than the difference in D retention.

(4) The co-deposit formed on the shadowed region of Tile 4 (Sample 4–10) in ILW-1 showed outstandingly high T concentration. The small but well detectable amount of T remained in the co-deposit even after heating in a vacuum to 1273 K for the TDS measurement. The analysis of chemical composition of the co-deposit using XPS indicated high C fraction at this particular position. Hence, the high T concentration and the presence of residue T after TDS measurement were ascribed to trapping of T by C. Such co-deposits with high C and T contents were not observed after ILW-3. It appears that the reduction of C impurity content in the vacuum vessel before starting DT operation is important to minimize T retention in ITER.

(5) The T retention in the W-coated CFC divertor tile after ILW-3 was higher than that after ILW-1. This observation was explained by the larger amount of T produced by DD fusion reactions due to larger number of shots and input energy in ILW-3.

(6) The T retention on the plasma-facing surfaces of the bulk W tile lamellae was negligibly small, while co-deposition of T with Be and O were observed on the side surfaces facing to toroidal and poloidal gaps. A part of O was present as OH, and hence it is plausible that a part of T was in the form of OT. No significant difference was observed between ion drift side and electron drift side, while the outboard side showed larger T retention than the inboard side.

## Declaration of Competing Interest

The authors declare that they have no known competing financial interests or personal relationships that could have appeared to influence the work reported in this paper.

## Acknowledgements

This work has been carried out within the framework of the EUROfusion Consortium and has received funding from the Euratom research and training programme 2014-2018 and 2019-2020 under grant agreement No 633053. The views and opinions expressed herein do not

necessarily reflect those of the European Commission. The study was supported by the ITER Broader Approach Activities and JSPS KAKENHI (Grant No. JP26289353).

## References


[1] M. Merola, F. Escourbiac, R. Raffray, P. Chappuis, T. Hirai, A. Martin, Overview and status of ITER internal components, Fusion Eng. Des. 89 (2014) 890–895, https://doi.org/10.1016/j.fusengdes.2014.01.055.

[2] T. Hirai, et al., R&D on full tungsten divertor and beryllium wall for JET ITER-like wall project, Fusion Eng. Des. 82 (2007) 1839–1845, https://doi.org/10.1016/j.fusengdes.2007.02.024.

[3] A. Widdowson, et al., Deposition of impurity metals during campaigns with the JET ITER-like wall, Nucl. Mater. Energy 19 (2019) 218–224, https://doi.org/10.1016/j.nme.2018.12.024.

[4] A. Widdowson, et al., Fuel inventory and material migration of JET main chamber plasma facing components compared over three operational periods, Phys. Scr. T171 (2020) 014051, https://doi.org/10.1088/1402-4896/ab5350.

[5] S. Brezinsek, et al., Fuel retention studies with the ITER-like wall in JET, Nucl. Fusion 53 (2013) 083023, https://doi.org/10.1088/0029-5515/53/8/083023.

[6] K. Heinola, et al., Fuel retention in JET ITER-like wall from post-mortem analysis, J. Nucl. Mater. 463 (2015) 961–965, https://doi.org/10.1016/j.jnucmat.2014.12.098.

[7] K. Heinola, et al., Long-term fuel retention in JET ITER-like wall, Phys. Scr. T167 (2016) 014075, https://doi.org/10.1088/0031-8949/T167/1/014075.

[8] A. Baron-Wiechec, et al., Global erosion and deposition patters in JET with the ITER-like wall, J. Nucl. Mater. 463 (2015) 157–161, https://doi.org/10.1016/j.jnucmat.2015.01.038.

[9] M. Mayer, et al., Erosion and deposition in the JET divertor during the second ITER-like wall campaign, Phys. Scr. T170 (2017) 014058, https://doi.org/10.1088/1402-4896/aa8ff9.

[10] M. Rubel, et al., Fuel inventory and deposition in castellated structures in JET-ILW, Nucl. Fusion 57 (2017) 066027, https://doi.org/10.1088/1741-4326/aa6864.

[11] A. Baron-Wiechec, et al., Thermal desorption spectrometry of beryllium plasma facing tiles exposed in the JET tokamak, Fusion Eng. Des. 133 (2018) 135–141, https://doi.org/10.1016/j.fusengdes.2018.05.075.

[12] A. Lahtinen, et al., Deuterium retention on the tungsten-coated divertor tiles of JET ITER-like wall in 2015–2016 campaign, Fusion Eng. Des. 146 (2019) 1979–1982, https://doi.org/10.1016/j.fusengdes.2019.03.081.

[13] J. Likonen, et al., Investigation of deuterium trapping and release in the JET divertor during the third ILW campaign using TDS, Nucl. Mater. Energy 19 (2019) 300–306, https://doi.org/10.1016/j.nme.2019.03.012.

[14] Y. Hatano, et al., 2D tritium distribution on tungsten tiles used in JET ITER-like wall project, J. Nucl. Mater. 463 (2015) 966–969, https://doi.org/10.1016/j.jnucmat.2014.12.041.

[15] Y. Hatano, et al., Tritium distributions on tungsten and carbon tiles used in the JET divertor, Phys. Scr. T167 (2016) 014009, https://doi.org/10.1088/0031-8949/T167/1/014009.

[16] Y. Hatano, et al., Tritium analysis of divertor tiles used in JET ITER-like wall campaigns by means of β-ray induced x-ray spectrometry, Phys. Scr. T170 (2017) 014014, https://doi.org/10.1088/1402-4896/aa8931.

[17] S. Masuzaki, et al., Analyses of microstructure, composition and retention of hydrogen isotopes in divertor tiles of JET with the ITER-like wall, Phys. Scr. T170 (2017) 014031, https://doi.org/10.1088/1402-4896/aa8bcc.

[18] Y. Hatano, et al., Tritium distributions on W-coated divertor tiles used in the third JET ITER-like wall campaign, Nucl. Mater. Energy 18 (2019) 258–261, https://doi.org/10.1016/j.nme.2019.01.001.

[19] M. Tokitani, et al., Surface morphology of the bulk tungsten divertor tiles from JET ITER-like wall, Phys. Scr. T171 (2020) 014010, https://doi.org/10.1088/1402-4896/ab3d09.

[20] S.E. Lee, et al., Tritium distribution analysis of Be limiter tiles from JET-ITER like wall campaigns using imaging plate technique and β-ray induced X-ray spectrometry, Fusion Eng. Des. 160 (2020) 111959, https://doi.org/10.1016/j.fusengdes.2020.111959.

[21] J. F. Ziegler, SRIM - The Stopping and Range of Ions in Matter, http://www.srim.org/. (current as of January 2, 2021).

[22] L. Katz, A.S. Penfold, Range-energy relations for electrons and the determination of beta-ray end-point energies by absorption, Rev. Mod. Phys. 24 (1952) 28–44, https://doi.org/10.1103/RevModPhys.24.28.

[23] J. H. Hubbell, S. M. Seltzer, the National Institute of Standards and Technology (NIST) Standard Reference Database 126 X-Ray Mass Attenuation Coefficients, https://www.nist.gov/pml/x-ray-mass-attenuation-coefficients. (current as of January 2, 2021).

[24] Y. Oya, et al., Correlation of surface chemical states with hydrogen isotope retention in divertor tiles of JET with ITER-Like Wall, Fusion Eng. Des. 132 (2018) 24–28, https://doi.org/10.1016/j.fusengdes.2018.04.124.

[25] Y. Oya, et al., Comparison of hydrogen isotope retention in divertor tiles of JET with the ITER-like wall following campaigns in 2011–2012 and 2015–2016, Fusion Sci. Technol. 76 (2020) 439–445, https://doi.org/10.1080/15361055.2020.1716455.

[26] M. Tokitani, et al., Micro-/nano-characterization of the surface structures on the divertor tiles from JET ITER-like wall, Fusion Eng. Des. 116 (2017) 1–4, https://doi.org/10.1016/j.fusengdes.2017.01.002.

[27] M. Tokitani, et al., Plasma-wall interaction on the divertor tiles of JET ITER-like wall from the viewpoint of micro/nanoscopic observations, Fusion Eng. Des. 136 (2018) 199–204, https://doi.org/10.1016/j.fusengdes.2018.01.051.

[28] I. Jepu, et al., Beryllium melting and erosion on the upper dump plates in JET during three ITER-like wall campaigns, Nucl. Fusion 59 (2019) 086009, https://doi.org/10.1088/1741-4326/ab2076.

[29] E. Pajuste, et al., Structure, tritium depth profile and desorption from 'plasma-facing' beryllium materials of ITER-like-wall at JET, Nucl. Mater. Energy 12 (2017) 642–647, https://doi.org/10.1016/j.nme.2017.03.017.

[30] E. Pajuste, et al., Comparison of the structure of the plasma-facing surface and tritium accumulation in beryllium tiles from JET ILW campaigns 2011–2012 and 2013–2014, Nucl. Mater. Energy 19 (2019) 131–136, https://doi.org/10.1016/j.nme.2019.02.011.

[31] T. Torikai et al., Tritium retention in dust particles and divertor tiles of JET operated with the ITER-like wall, 28th IAEA Fusion Energy Conference, Contribution ID: 839. https://conferences.iaea.org/event/214/contributions/17656/. (current as of August 15, 2020).

[32] Y. Oya, et al., Effect of carbon impurity reduction on hydrogen isotope retention in QUEST high temperature wall, Fusion Eng. Des. 146 (2019) 1480–1484, https://doi.org/10.1016/j.fusengdes.2019.02.110.

[33] N. Yoshida et al., private communication.